Thermodynamics and Theory of External and Internal Oxidation of Alloys

Article · December 2010

DOI: 10.1016/B978-044452787-5.00012-3

1 author:

Brian M Gleeson
University of Pittsburgh
188 PUBLICATIONS **5,391** CITATIONS

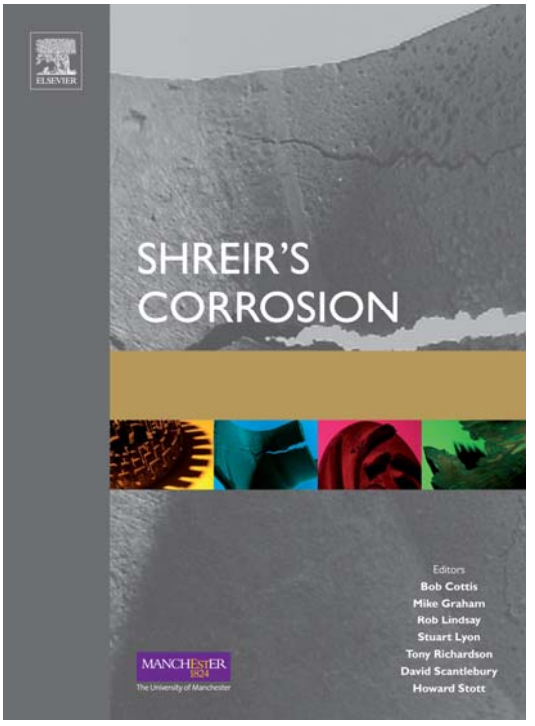

Gleeson B 2010 Thermodynamics and Theory of External and Internal Oxidation of Alloys. In: Richardson J A et al. (eds.) Shreir's Corrosion, volume 1, pp. 180-194 Amsterdam: Elsevier.

1.09 Thermodynamics and Theory of External and Internal Oxidation of Alloys

B. Gleeson
Department of Mechanical Engineering and Materials Science, The University of Pittsburgh, 647 Benedum Hall, Pittsburgh, PA 15261, USA

Symbols

a_i Chemical activity of phase or component i
D_i Diffusion coefficient of component i ($m^2\ s^{-1}$)
K Equilibrium constant for a given reaction
k_l Linear rate constant ($m\ s^{-1}$) or ($kg\ m^{-2}\ s^{-1}$)
k_p Parabolic rate constant ($m^2\ s^{-1}$) or ($kg^2\ m^{-4}\ s^{-1}$)
N_i Mole fraction of component i
P_i Partial pressure of gaseous species i
R Universal gas constant (8.314 $J\ mol^{-1}\ K^{-1}$)
T Temperature (K)
t Time (s)
V_m Molar volume of metal or alloy ($m^3\ mol^{-1}$)
X Thickness of metal consumed due to scaling (m)
x Scale thickness (m)
ΔG° Gibbs free enthalpy in the standard state ($J\ mol^{-1}$)
ΔW Weight change ($kg\ m^{-2}$)
γ_i Chemical activity coefficient of solute i
ν Stoichiometric factor for the oxide BO_ν

1.09.1 Introduction

High temperature corrosion plays an important role in the selection of materials in modern industry. Numerous commercial processes such as electric power generating plants, aerospace, gas turbines, heat-treating, and mineral and metallurgical processing operate at temperatures exceeding ~500°C.[1] Oxidation is often the most important high temperature corrosion reaction in these commercial processes. Indeed, most high temperature alloys are designed to react with the oxidizing environment in such a way that a protective oxide scale forms.[2] The degradation resistance of a high temperature alloy depends on sustaining the formation of this protective scale.

The properties of the scale determine the extent to which protection can be provided. Ideally, the scale should exhibit a slow growth rate, good adherence to the alloy substrate, a high stability, and be continuous and free of defects such as microcracks or large

Shreir's Corrosion, Fourth Edition (2010), vol. 1, pp. 180-194

voids. In general, a chromia, alumina, or silica scale can meet these requirements for high temperature oxidation resistance, with chromia-forming alloys being the most extensively used in high temperature industrial applications.

Almost all theoretical treatments of high temperature corrosion assume local equilibrium. In the majority of cases, this proves to be a reasonable assumption, although it is usually insufficient for predicting the nature and phase constitution of the reaction product. This is because reaction kinetics dictate the pathway for scale development. The following discusses key fundamental aspects associated with the thermodynamics and kinetics of high temperature corrosion. From a thermodynamic standpoint, it will be shown that relative partial pressures of the gaseous components in the reacting atmosphere are important for predicting the composition of the product scale. From a kinetic standpoint, it will be shown that limiting equations can be established for predicting both scaling kinetics and critical concentrations in the alloy for transitioning to and sustaining protective scaling behavior.

1.09.2 Pure Metal Reactions

In the context of this discussion, the metal and gas react to form a solid surface scale. The prototypical gas will be oxygen; however, it should be realized that the fundamental treatments equally apply to other gases, such as sulfur and nitrogen. Moreover, the oxidant may be simple, like O_2, S_2, and N_2, or it may be more complex, like H_2O, H_2S, and NH_4. For the sake of clarity, the following discussion will consider oxide-scale formation. An oxide scale may be a single layer or it may be comprised of two or more layers of varying compositions that depend on the temperature and oxidizing conditions. There are two important factors in discussing the oxidation of metals: thermodynamics and kinetics. Metallic elements react with oxygen to form oxides if it is energetically feasible. Thermodynamics show whether or not a reaction can take place. When the oxidation reaction is possible, kinetics shows how fast the reaction will be. In practical applications, kinetics is of more importance because it determines the extent of metal consumption and the overall reaction pathway (i.e., assemblage and structure of the reaction product). Oxidation theory of pure metals provides the foundation for understanding the more complicated processes associated with alloy oxidation.

1.09.2.1 Thermodynamics of a Single-Oxidant Reaction

Consider the high temperature reaction of a metal, M, with an oxidant gas, in this case oxygen. The metal initially absorbs oxygen and then chemical reaction ensues to form an oxide. For the metals of relevance to this review, the resulting oxide is solid. Thus, the oxide first nucleates and then grows to form a scale on the metal surface. Depending on its growth kinetics, the scale may or may not protect the underlying metal.

The formation of an oxide may be generally described by the reaction

$$\frac{2x}{y}\mathrm{M} + \mathrm{O_2} = \frac{2}{y}\mathrm{M}_x\mathrm{O}_y \qquad [1]$$

Presented in this manner, the high temperature oxidation of metals may seem to be among the simplest of reactions; however, the reaction path and behavior often involve a number of phenomena and processes that depend on a variety of factors.[3,4] In fact, at the same temperature for a given gas–metal reaction, one can observe drastically different rates of reaction (linear, parabolic, or any other rate) when the gaseous composition of the atmosphere is altered and the relative partial pressures of the gaseous components are different.[5]

Under equilibrium conditions, the law of mass action for reaction [1] gives[6]

$$K_1 = \frac{a_{\mathrm{M}_x\mathrm{O}_y}^{2/y}}{a_{\mathrm{M}}^{2x/y}\, a_{\mathrm{O_2}}} \qquad [2]$$

where K_1 is the temperature-dependent equilibrium constant and a_i is the chemical activity of species i. In most cases, the solids (metal and oxide) are assumed to be in their pure standard state, so that their activities are defined as unity. At relatively high temperatures and moderate pressures, the oxidant gas can be treated as being ideal; that is, the activity of oxygen can be approximated by its partial pressure in atmospheres. Thus, eqn [2] simplifies to

$$K_1 = 1/P_{\mathrm{O_2}} \qquad [3]$$

where $P_{\mathrm{O_2}}$ is the oxygen partial pressure.

Thermodynamically, reaction [1] for any metal can take place spontaneously from left to right when its overall Gibbs free energy change, ΔG, is negative. For reaction [1], the Gibbs free energy change under isobaric conditions is given as:

$$\Delta G = \Delta G^\circ + RT\ \ln K_1 \qquad [4]$$

where ΔG° is the standard Gibbs free energy of formation of the oxide at absolute temperature

T and R is the gas constant. If $\Delta G = 0$, the system is at equilibrium, and if $\Delta G > 0$, the reaction is thermodynamically unfavorable. At equilibrium ($\Delta G = 0$),

$$\Delta G^\circ = -RT \ln K_1 = RT \ln P_{O_2} \quad [5]$$

Thus, knowing that at equilibrium both the forward and reverse reaction rates are equal, the dissociation pressure of the oxide can be defined from [5] as:

$$P_{O_2}^{diss} = \exp\left(\frac{\Delta G^\circ}{RT}\right) \quad [6]$$

The metal M can only be oxidized to the oxide M_xO_y at the temperature T if the ambient partial pressure of oxygen is larger than the dissociation pressure defined by eqn [6].

For the usual conditions of constant temperature and pressure, the auxiliary function ΔG° is usually described by the simple relation

$$\Delta G^\circ = \Delta H^\circ - T\Delta S^\circ \quad [7]$$

where ΔH° is the enthalpy of reaction and ΔS° is the entropy change under standard-state conditions. Tabulated values of ΔH° and ΔS° for the determination of ΔG° at any given temperature are readily available.[7–9] A small selection of useful values is given in **Table 1**.

Equation [7] shows that a plot of ΔG° versus T gives a straight line. This line would change in slope when a new phase forms (i.e., at melting or boiling temperature). A Gibbs energy–temperature diagram, usually called an Ellingham diagram,[6] summarizes the temperature dependence of ΔG° for various common oxidation reactions at a standard state ($p_{O_2} = 1$ atm). Such a diagram is shown in **Figure 1** for oxides.

Table 1 Standard energies of reaction[7,8] for pure solid metal (except liquid Al) and various common gasses

Reaction	$\Delta G^\circ = \Delta H^\circ - T\Delta S^\circ$ ($J\,mol^{-1}$)	
	ΔH° ($J\,mol^{-1}$)	$-\Delta S^\circ$ ($J\,mol^{-1}\,K$)
$\frac{2}{3}Al(l) + \frac{1}{2}O_2 = \frac{1}{3}Al_2O_2$	−565 900	128
$Co + \frac{1}{2}O_2 = CoO$	−233 886	70.7
$3CoO + \frac{1}{2}O_2 = Co_2O_4$	−183 260	148.1
$\frac{2}{3}Cr + \frac{1}{2}O_2 = \frac{1}{3}Cr_2O_2$	−373 420	86
$Fe + \frac{1}{2}O_2 = FeO$	−264 890	65.4
$3FeO + \frac{1}{2}O_2 = Fe_2O_4$	−312 210	125.1
$2Fe_2O_4 + \frac{1}{2}O_2 = 3Fe_2O_2$	−249 450	140.7
$Mn + \frac{1}{2}O_2 = MnO$	−412 304	72.8
$Ni + \frac{1}{2}O_2 = NiO$	−234 345	84.3
$\frac{1}{2}Si + \frac{1}{2}O_2 = \frac{1}{2}SiO_2$	−451 040	86.8
$H_2 + \frac{1}{2}O_2 = H_2O$	−246 440	54.8
$CO + \frac{1}{2}O_2 = CO_2$	−282 420	86.8
$O_2 + \frac{1}{2}S_2 = SO_2$	−362 420	72.4
$NiO + Cr_2O_2 = NiCr_2O_4$	−1 376 880	332
$NiO + Al_2O_2 = NiAl_2O_4$	−1 933 667	408

The calculated ΔG° value would be for the mole numbers shown in the particular reaction considered.

The Ellingham diagram in **Figure 1** shows the relative thermodynamic stability of the indicated oxides. The lower the line on the diagram, the more negative the standard free energy of formation and, hence, the more stable the oxide. For example, the lines for Al_2O_3, SiO_2, and Cr_2O_3 are lower than those for FeO, NiO, and CoO in the Ellingham diagram, so the former oxides are more stable and therefore meet an important criterion for being protective scales. It is further seen in **Figure 1** that the ΔG° versus T lines for most of the oxides are parallel and positively sloped. This is a consequence of the fact that the entropy of a gas is much larger than that of a solid. Thus, for the metal oxidation reactions represented by eqn [1],

$$\Delta S^\circ = \frac{2}{y} S^\circ_{M_xO_y} - \frac{2x}{y} S^\circ_M - S^\circ_{O_2} \approx -S^\circ_{O_2}. \quad [8]$$

It follows from eqn [7] that $\partial\Delta G^\circ/\partial T = -\Delta S^\circ \approx S^\circ_{O_2}$, which is greater than zero.

The P_{O_2} can be read directly from **Figure 1** by using the P_{O_2} scale along the bottom and the right side of the diagram. A straight line drawn from the index point labeled 'O' (at $\Delta G^\circ = 0$, $T = 0$ K) at the upper left of the diagram, through a specific temperature point on an oxide line, intersects the P_{O_2} scale at the dissociation oxygen partial pressure ($P_{O_2}^{diss}$) for that oxide at that particular temperature. Accordingly, the oxides lower on the diagram are more stable and consequently have lower $P_{O_2}^{diss}$ values. For instance, from **Figure 1**, it is found that the dissociation pressure for NiO is $\sim 10^{-10}$ atm at 1000°C, while that for Cr_2O_3 is $\sim 10^{-22}$ atm, and for SiO_2 and Al_2O_3, it is 10^{-26} and 10^{-34} atm, respectively. The significance of this is that it is difficult thermodynamically to preclude the oxidation of Cr, Si, and Al.

Similar free-energy diagrams, which can be interpreted in exactly the same way, have been constructed for sulfides, carbides, and nitrides.[5] Moreover, Lou *et al.*[10] presented an excellent review on the use of Ellingham diagrams for treating gas–solid reactions.

Low oxygen partial pressures are in practice achieved using oxygen-bearing gas mixtures. The most common gas mixtures are H_2O/H_2 and CO_2/CO. The partial pressures of oxygen are then established from the equilibria:

$$H_2O = H_2 + \frac{1}{2}O_2; K_9 = \frac{P_{H_2} P_{O_2}^{1/2}}{P_{H_2O}} \quad [9]$$

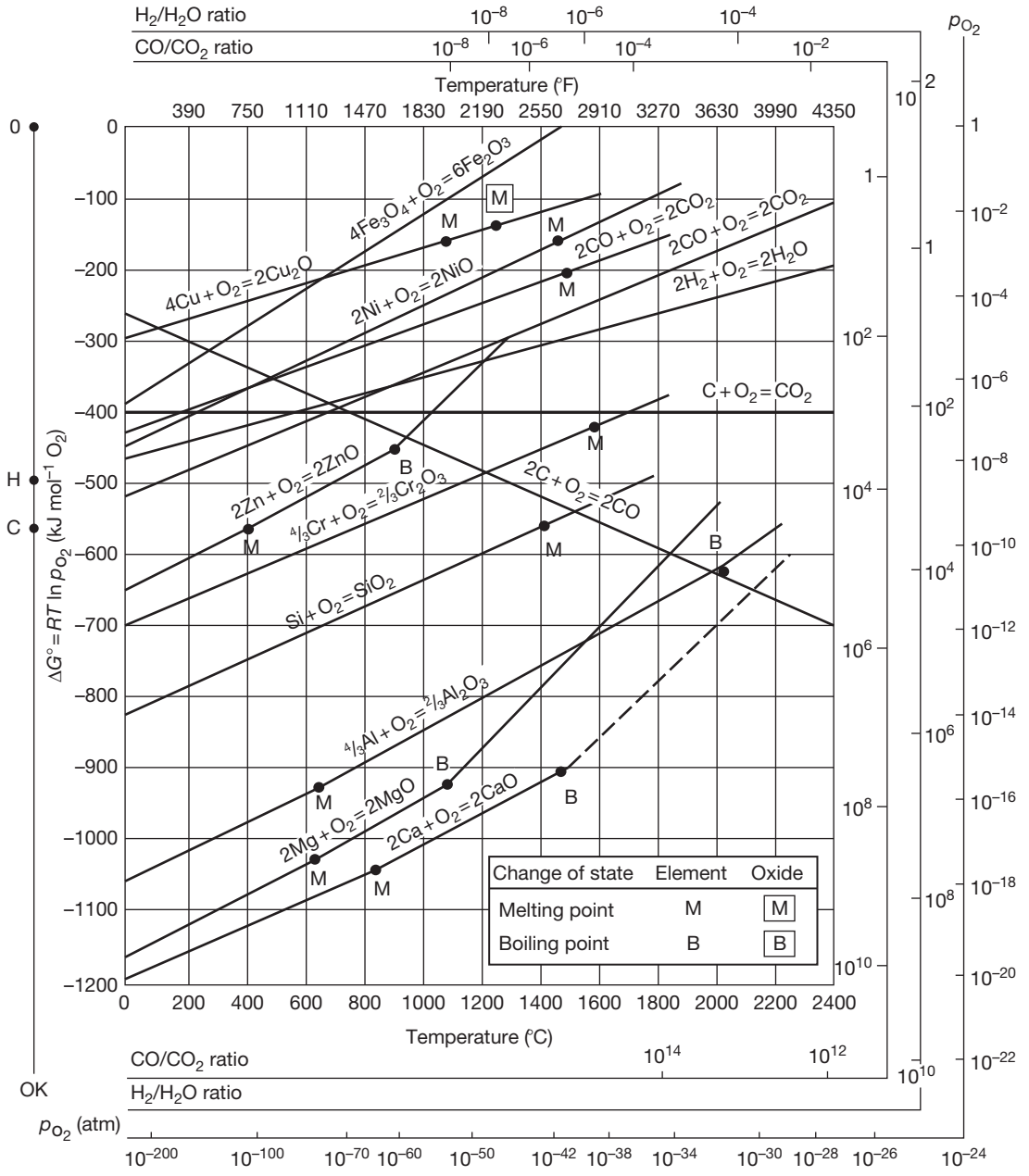

Figure 1 Ellingham diagram showing the standard Gibbs energies of formation of selected oxides as a function of temperature. Reproduced from Gaskall, D. R. *Introduction to the Thermodynamics of Materials*, 5th ed.; Taylor & Francis: New York, 2008.

and

$$CO_2 = CO + \frac{1}{2}O_2; K_{10} = \frac{P_{CO}P_{O_2}^{1/2}}{P_{CO_2}} \qquad [10]$$

where K_9 and K_{10} are the temperature-dependent equilibrium constants for reactions [9] and [10], respectively. Thus, the P_{O_2} may be determined from these equilibrium constants if the equilibrium P_{CO}/P_{CO_2} or P_{H_2}/P_{H_2O} ratios are known. In oxygen-lean gases containing both H_2O and CO_2, the P_{O_2} is usually determined by the H_2–H_2O reaction [9] since steam is more reactive than CO_2. Moreover, for a controlled laboratory experiment, it is preferred practice to facilitate the equilibrium by using a

platinum-containing catalyst in the reaction zone of the furnace.

In addition to the direct oxidation with oxygen, the overall metal oxidation reactions in these gas mixtures are:

$$xM + yH_2O = M_xO_y + yH_2 \qquad [11a]$$

and

$$xM + yCO_2 = M_xO_y + yCO \qquad [11b]$$

From **Figure 1**, the H_2/H_2O and CO/CO_2 ratios can be obtained by using the same method as for determining $P_{O_2}^{diss}$, using the index points labeled 'H' and 'C' at the left of the diagram instead of point 'O.'

The growth of a scale is usually sufficiently slow for local equilibrium to be closely approached. In fact, it is found that the Gibbs phase rule[6] can be applied to rationalizing the phase assemblage of a growing scale. Specifically, the Gibbs phase rule under isothermal and isobaric conditions is given as

$$P + F = C \qquad [12]$$

where P is the number of phases at a given location in the scale, F represents the degrees of freedom, and C number of components in the system. For the oxidation of a pure metal, $C = 2$ (i.e., metal and oxygen), and for diffusion to occur there must be a gradient in the chemical activity across the scale, so that $F = 1$. Thus, $P = 1$, meaning that only one phase can exist at a given plane (parallel to the metal/scale interface) within the scale. In practical terms, this means that a metal capable of forming multiple oxides must form those oxides as distinct scale layers. For example, at 1 atm O_2 and temperatures above 560 °C, pure iron oxidizes to form a triple-layered scale in the sequence $Fe|FeO|\ Fe_3O_4\ |Fe_2O_3\ |O_2$, with the oxide position being dictated by the necessity for the oxygen content to progressively increase when traversing from the iron to the oxygen at the scale surface. A similar line of reasoning can be used to show that a pure metal oxidized isothermally will not form internal oxide precipitates, but instead must form an external product.

1.09.2.2 Thermodynamics of Dual Oxidant Reactions

The thermodynamic aspects of multioxidant corrosion have been discussed by Giggins and Pettit.[11] Often, however, the complexity of a given process environment precludes an accurate determination of which type of corrosion should predominate. In such cases, it may be necessary to conduct field-exposure tests to properly evaluate the corrosion behavior of the candidate alloys. Even so, the assumption of thermodynamic equilibrium provides a reasonable starting point for assessment.

Quite often, two-dimensional phase stability diagrams are used to assess the high temperature corrosion of a metal M exposed to a dual-oxidant atmosphere. To illustrate this, the possible reactions of M exposed to oxidizing–sulfidizing atmosphere are determined by considering the following:

$$M + \frac{1}{2}O_2 \leftrightarrow MO \qquad [13]$$

$$M + \frac{1}{2}S_2 \leftrightarrow MS \qquad [14]$$

$$MO + \frac{1}{2}S_2 \leftrightarrow MS + \frac{1}{2}O_2 \qquad [15]$$

The equilibrium from reactions [13] and [14] defines the critical $P^*_{O_2}$ and $P^*_{S_2}$ values (i.e., dissociation pressures) for M/MO and M/MS equilibrium, respectively, while reaction [15] defines critical P_{S_2}/P_{O_2} ratios for MS/MO equilibria. With regard to the latter, it can be easily shown for reaction [15] that $\log(P_{S_2}) = \log(P_{O_2}) - 2\log K_{15}$, where K_{15} is the equilibrium constant for this reaction. Thus, a plot of $\log(P_{S_2})$ versus $\log(P_{O_2})$ should have a line of slope equal to the unity that separates MS stability from MO stability. **Figure 2** shows the general construction of an M–S–O phase-stability diagram. It is noted that a more complete diagram may include higher-order oxides and sulfides, as well as sulfates (MSO_4).[11] Only the simpler diagram is discussed here since the main important points can still be made.

The diagram in **Figure 1** shows the stability range of a metal and its oxide and sulfide products as a function of the two principal reactants: oxygen and

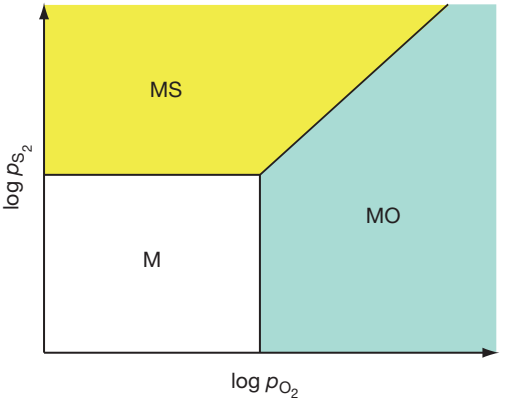

Figure 2 Schematic representation of a simple phase-stability diagram for a metal and its oxide and sulfide.

sulfur. A given atmosphere is defined by either equilibrium or nonequilibrium P_{O_2} and P_{S_2} values and would therefore be represented by a point in the stability diagram. The location of that point identifies the phase that is in stable equilibrium with that particular atmosphere. However, as shown in **Figure 3**, other phases can form even if only oxide stability is predicted. This depends on the reacting gas, the P_{O_2}–P_{S_2} combination, and whether the scale develops open pathways for gaseous penetration (e.g., microcracks). Internal sulfidation is particularly apt to occur in SO_2-containing atmospheres due to the local equilibrium dictated by the reaction $O_2 + \frac{1}{2} S_2 \rightarrow SO_2$, which has an equilibrium constant denoted as K_3. As indicated in **Figure 3**, the formation of an internal sulfide beneath an external oxide scale can only be completely avoided if

$$P_{SO_2} < K_3 P^*_{O_2} \sqrt{P^*_{S_2}} \qquad [16]$$

Although phase-stability diagrams are very useful for interpreting reaction products and gaining insights into reaction pathways, they do not have any predictive capabilities from a practical standpoint.

On the basis of equilibrium thermodynamics of reaction [15], the transition from sulfidation to oxidation of metal M should occur when

$$\left(\frac{P_{O_2}}{P_{S_2}}\right)^{1/2} > K_{15} \qquad [17]$$

The thermodynamic boundary separating sulfide and oxide stability in a phase stability diagram is determined by replacing '>' with '=' in eqn [17]. **Figure 4** shows the phase-stability diagram for the Type 310 stainless steel at 875 °C.[12] Superimposed on this diagram are experimental data indicating the type of scale formed on 310 under different P_{O_2}–P_{S_2} combinations. It is seen that sulfide-to-oxide transition at a given P_{S_2} actually occurs at a higher P_{O_2} than that predicted from equilibrium calculations. The experimentally-determined boundary is dictated by kinetic factors and, accordingly, is referred to as the kinetic boundary. For the case of the 310 stainless steel shown in **Figure 4**, the actual P_{O_2} values for the transition from chromium–sulfide to chromium–oxide formation are about three orders of magnitude higher than the equilibrium values. The kinetic factors which influence the location of the kinetic boundary include composition and surface finish of the alloy, and gas composition. Although theoretical prediction of the location of a kinetic boundary is not possible, LaBranche and Yurek[13] showed that for H_2–H_2O–H_2S gas mixtures there is a critical H_2O/H_2S ratio associated with the kinetic boundary. The value of this ratio is dictated by the competitive formation of the oxide and the faster-growing sulfide. It was found by LaBranche and Yurek that oxide formation on pure chromium at 900°C could only occur when the area fraction of Cr_2O_3 was greater than ~0.9 in the early stages of exposure, which corresponds to $H_2O/H_2S > 10$.

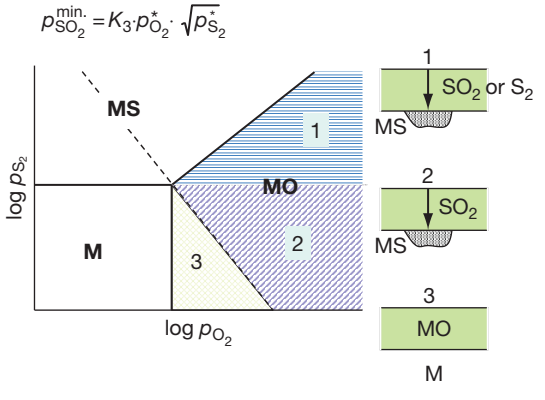

Figure 3 Application of the phase-stability diagram in identifying possible modes of attack.

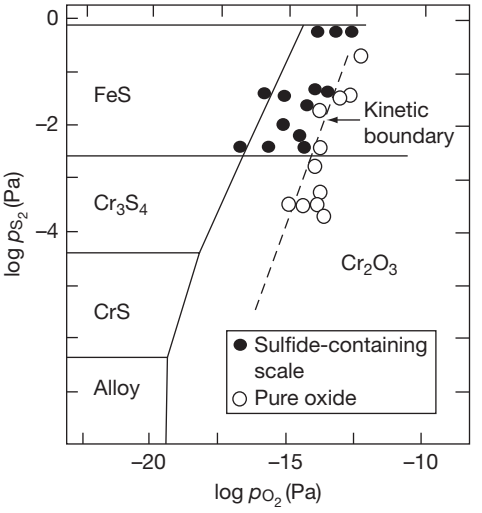

Figure 4 Thermodynamic phase-stability diagram for type 310 stainless steel at 875°C, showing the experimentally-determined kinetic boundary. Reproduced from Stroosnijder, M. F.; Quadakkers, W. J. *High Temp. Technol*. **1986**, *4*, 141.

1.09.2.3 Kinetics of Scale Formation

The reaction of a metal with an oxidant to form a product scale is concomitant with a weight gain due to pick-up of the oxidant (e.g., grams of oxygen gained). Accordingly, the scaling rate may be quantified by the change in the scale thickness, x (cm), or by weight gain, ΔW (mg cm^{-2}). In the case of oxidation, these two parameters are directly related by

$$x = \frac{V_{ox}}{yM_O}\Delta W \qquad [18]$$

where V_{ox} is the molar volume of oxide in cm^3 mol^{-1}, y is the stoichiometric amount of oxygen in oxide M_xO_y, and M_o is the atomic weight of oxygen.

The formation of oxide scale is also related to the consumption of metal, and the relationship between ΔW and the thickness of the metal consumed (X) is given by

$$X = \frac{V_m}{\gamma M_O}\Delta W \qquad [19]$$

where V_m is the molar volume of metal in cm^3 mol^{-1} and γ is the stoichiometric factor for the oxide scale product (i.e., $\gamma = y/x$ for M_xO_y). For most metals, the oxidation rates follow one or more of the three possible kinetic laws: linear, logarithmic, and parabolic. These kinetic laws are discussed in the following.

Formation of an oxide scale will separate the two reactants, metal and gaseous oxygen. In order for the reaction to proceed further, at least one of the reactants must progress through the scale to form more oxide at the oxide/gas, oxide/metal, or both interfaces. The mechanisms by which the reactants progress through the scale can therefore be an important part of the overall mechanism and kinetics by which high temperature oxidation reaction proceeds. Another aspect of the oxidation process, which can sometimes be rate controlling, is the kinetics of the interfacial reaction steps.

1.09.2.3.1 Parabolic rate law

At high temperature, initial scale growth is usually very rapid; however, the reaction rate will eventually decrease when scale thickness reaches ~0.5 μm and the transport of reacting species through the scale becomes rate controlling. When the rate-controlling step in the oxidation process is the diffusion of reactant(s) through the oxide layer and with the boundary conditions for diffusion being time independent, the scaling kinetics will follow the parabolic rate law. Parabolic kinetics results from the fact that the scale thickness, x, increases with time, t, and, since this corresponds to the increasing diffusion distance, the oxidation rate decreases. Thus, the instantaneous oxidation rate is quite simply inversely proportional to the oxide thickness, that is,

$$\frac{dx}{dt} = \frac{k_p'}{x} \qquad [20]$$

where k_p' is a proportionality constant. Integration of eqn [20] gives

$$x^2 = k_p t + C \qquad [21]$$

where k_p is taken to be the parabolic rate constant ($k_p = 2\,k_p'$) with typical units of cm^2 s^{-1}. Another form of the parabolic rate equation is given by the weight gain (g cm^{-2}):

$$\Delta W^2 = k_p t + C \qquad [22]$$

where the units of k_p in this case are g^2 cm^{-4} s.

The parabolic rate law is the standard for analysis of high temperature oxidation kinetics, in which diffusion through the relatively thick scale controls reaction rates. The diffusion-controlled scale-thickening process is thermally activated, meaning that the rate increases exponentially with temperature, as given by the Arrhenius equation:

$$k_p = k_o \exp\left(\frac{-Q}{RT}\right) \qquad [23]$$

Here, k_o is a constant that is a function of the oxide composition and the gas pressure, and Q is the activation energy for oxide-scale growth. **Figure 5**[1] shows the temperature dependence of the k_p values for the oxides of Fe, Co, Ni, Cr, Al, and Si. The figure shows a range of k_p values for Al_2O_3 and Cr_2O_3 growth because these oxides do not show intrinsic behavior and are instead very sensitive to impurities (i.e., doping).

Deviations from parabolic kinetics are generally analyzed in terms of chemical and metallurgical effects on the rates of the relevant diffusing process(es). The parabolic rate law will not hold in the very early stages of oxidation, before the scale has developed sufficient continuity and thickness. In the case of hafnium and zirconium, the time exponent in eqn [21] is found to be ~3 (cubic kinetics) rather than 2 (parabolic kinetics) at high temperatures. This has been attributed to the simultaneous dissolution of oxygen into the substrate metal during oxidation.[14] It has also been shown for NiO-[15] and Al_2O_3-scale[16] growth that subparabolic kinetics can occur if both short-circuit diffusion through the scale predominates and the average grain size of the scale increases with oxidation time.

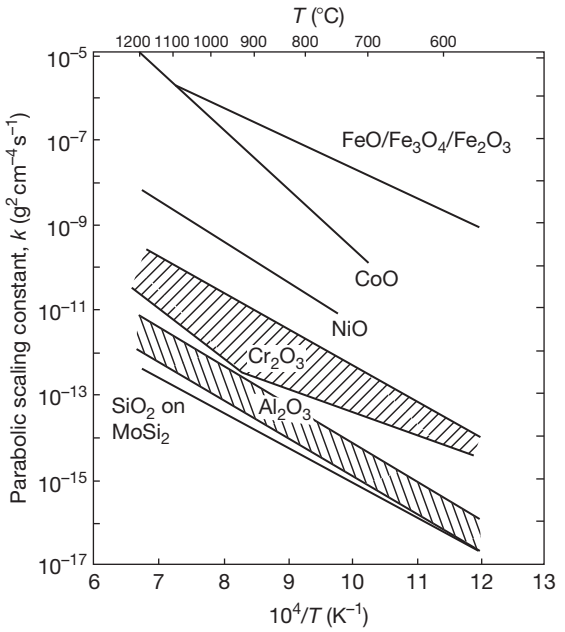

Figure 5 Parabolic oxidation rate constant for various oxide scales as a function of temperature. Reproduced from Gleeson, B. In *Corrosion and Environmental Degradation*, *Vol. II*: Volume 19 of the Materials Science and Technology Series; Schütze, M., Ed.; Wiley-VCH: Weinheim, Germany, 2000.

1.09.2.3.2 Linear rate law

Under certain conditions, the oxidation of a metal proceeds at a constant rate according to a linear rate law, that is,

$$x = k_l t \qquad [24]$$

where x is the scale thickness and k_l is the linear rate constant. A linear rate law may result when a phase-boundary reaction controls the kinetics rather than a transport process. An example is CO_2 dissociation at the scale surface controlling the oxidation kinetics of steel in a CO_2-rich atmosphere.[17]

Linear kinetics is also possible if the oxide is volatile or molten, if the scale spalls or cracks, or if a porous, nonprotective oxide forms on the metal.[4] Since the rate of oxidation never slows down, consumption of the metal occurs in a relatively short time in comparison to a metal scaling according to parabolic kinetics. Examples of metals that scale in a nonprotective, linear manner due to continual scale cracking are Nb and Ta.[18]

In the early stages of a metal oxidation process, the scale may be sufficiently thin that linear oxidation kinetics prevails. As the scale thickens, a transition to parabolic kinetics will usually ensue.[19] Conversely, microcracking and porosity may develop as the scale thickens, reducing the protectiveness of the oxide. The parabolic rate law may then fail, and the kinetics approaches linearity at some time after the start of reaction and scale growth. That is, a constant oxidation rate can develop after a period of parabolic behavior. In this special case of parabolic scaling superimposed on a relatively constant rate of scale cracking and healing, the overall kinetics is said to be 'paralinear.'[20]

1.09.2.3.3 Logarithmic rate law

At low temperatures (e.g., $T < 300$–$400\,^{\circ}C$), oxidation rates are often inversely proportional to time, that is,

$$\frac{dx}{dt} = \frac{k}{t} \qquad [25]$$

where k is a constant. Integration of [25] leads to the logarithmic rate law

$$x = k_a \log(k_b t + 1) \qquad [26]$$

where k_a and k_b are constants. Logarithmic oxidation is usually obeyed for relatively thin scales at low temperatures.

1.09.2.4 Transport Properties of Metal Oxides

Metallic oxides are seldom stoichiometric, meaning that the metal-to-oxygen atom ratio is not exactly that given by the stoichiometric chemical formula, even though the compound is electrically neutral. The same can be stated for sulfides and nitrides, but the focus here will be on oxides as the prototypical systems. The ionic charge imbalance in a nonstoichiometric oxide is compensated by electronic charges, that is, electron and electron holes. As a consequence, nonstoichiometric oxides exhibit both electronic and ionic conductivities. These conductivities are temperature dependent, which, from the electronic standpoint, classifies the nonstoichiometric oxides as semiconductors.

Electronic semiconductors are categorized as n-type (excess of electrons) or p-type (excess of electron holes). The n-type oxides may have either an excess of cation interstitials or an excess of oxygen vacancies (i.e., a deficiency in filled sites on the oxygen sublattice, MO_{1-x}) as the principal ionic defects. Some examples of n-type oxides are TiO_2, Fe_2O_3, $NiFe_2O_4$, ZnO, Al_2O_3, and SiO_2.[18] For n-type oxides, the principal ionic defect concentration, C, is found to be proportional to the negative power of the oxygen partial pressure[21]:

$$C \propto P_{O_2}^{-1/n} \quad [27]$$

where n is a positive integer which depends upon the charge of the ionic defect in the oxide and the oxide's stoichiometry.

The p-type oxides may have either an excess of cation vacancies (i.e., a deficiency in filled sites on the metal sublattice, $M_{1-x}O$) or an excess of oxygen interstitials. Some common p-type oxides include NiO, CoO, FeO, $FeCr_2O_4$, $CoCr_2O_4$, and $NiAl_2O_4$. For p-type oxides, the principal ionic defect concentration is related to the oxygen partial pressure by[21]:

$$C \propto P_{O_2}^{1/n} \quad [28]$$

During the oxidation process, ions transport by two ways: the cation migrates outward to scale/gas interface and the anion migrates inward to metal/scale interface (**Figure 6**). Thus, two reactions could potentially happen at the two interfaces to result in scale growth, although it is typically found that one reaction predominates. In other words, either metal or oxygen diffusion predominates in the thickening of a given oxide scale.

For the defective structures treated so far, it has been assumed that the oxides are pure; however, it is thermodynamically impossible to produce perfectly pure compounds or materials. It is therefore necessary to consider the effects of impurities on the defective structure of oxides. It is noted, however, that the presence of impurities can sometimes be neglected if the intrinsic defect concentration in the host oxide is relatively large. As an example of the so-called 'doping effect,'[21] the following is found for a p-type, metal-deficient oxide $M_{1-x}O$:

- The addition of substitutionally dissolved foreign cations of lower valence increases the concentration of electron holes and decreases the concentration of cation vacancies.
- The addition of substitutionally dissolved foreign cations of higher valence decreases the concentration of electron holes and increases the concentration of cation vacancies.

Thus, for the p-type, metal-deficient NiO, doping with Cr^{3+}, will cause an increase in the nickel vacancy concentration, which in turn will cause an increase in the effective diffusivity of nickel in the NiO. This increase in diffusivity is manifested as an increase in the k_p for NiO-scale growth. Indeed, it is found experimentally that NiO grows faster on dilute Ni–Cr alloys than on pure Ni.[22]

1.09.2.5 Wagner's Theory of Metal Oxidation

Carl Wagner's theory of metal oxidation[23,24] provides a fundamental understanding of the essential features of the high temperature growth of a continuous scale. The model ideally assumes that the scale is dense, single-phase, continuous, and adheres to the metal over the entire metal surface. The basic assumption of the theory is that lattice diffusion of the reacting atoms or ions through the dense scale is rate controlling (i.e., the microstructure of the oxide scale was not considered). **Figure 7** gives a set-up of the model.[14]

As indicated in **Figure 7**, the scale growth involves fluxes of both ionic and electronic charged species. The driving forces for these fluxes are related to the chemical potential gradient and electrostatic field that develop in the growing scale. The relative

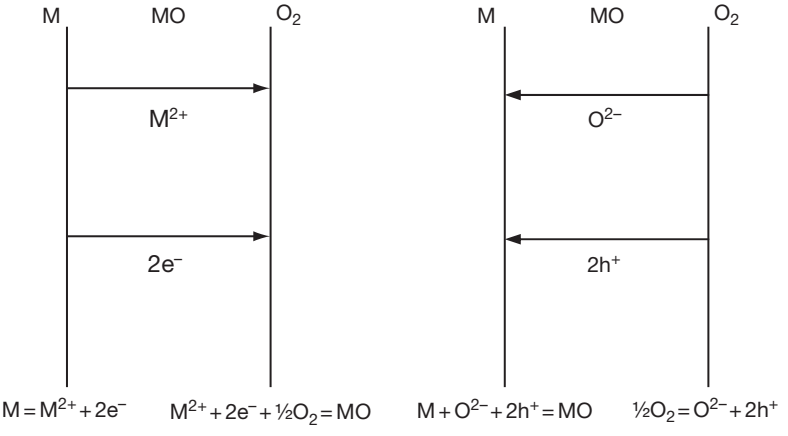

Figure 6 Ionic and electronic transport processes and interfacial reactions in the growth of a nonstoichiometric oxide scale MO.

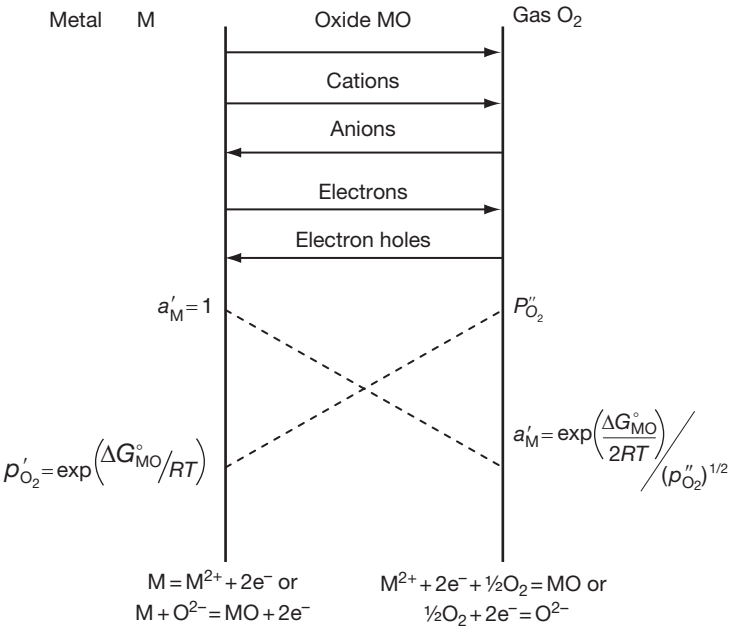

Figure 7 Transport processes according to Wagner's theory. Adopted from Birks, N.; Meier, G. H. *Introduction to High Temperature Oxidation of Metals*; Edward Arnold: London, 1983.

migration rates of cations, anions, electrons, and electron holes must also be balanced such that no net charge build up occurs within the scale.

Wagner derived an expression for the parabolic rate constant in terms of the electronic and ionic conductivities of the oxide or, alternatively, in terms of the self-diffusion coefficients of the reacting ions in which parameters can be measured relatively easily. Limiting cases of Wagner's derivation are as follows[14]:

$$k' = \frac{1}{RT}\int_{\mu''_M}^{\mu'_M} D_M \, d\mu_M \qquad [29]$$

and

$$k' = \frac{1}{RT}\int_{\mu''_X}^{\mu'_X} D_X \, d\mu_X \qquad [30]$$

where k' is the parabolic rate constant with units of cm^2s^{-1}, D_M and D_X are the self-diffusion coefficients for metal, M, and nonmetal, X, through the scale, respectively, and μ_M and μ_X are the chemical potentials for the metal and nonmetal. Equation [29] is valid when cation diffusion predominates and eqn [30] is valid when anion diffusion predominates. The good agreement between parabolic rate constants calculated from diffusivities and the oxidation rate constants measured experimentally have provided validation for Wagner's theory.[25,26]

Because the diffusion flux within the oxide is proportional to the defect concentration, eqn [28] can be used for a p-type oxide to arrive at the following relation for the oxidation rate:

$$k' \propto [(P^o_{O_2})^{1/n} - (P^i_{O_2})^{1/n}] \qquad [31a]$$

where $P^o_{O_2}$ and $P^i_{O_2}$ are the oxygen pressures at the scale/gas interface and metal/scale interface respectively, and n is an integer related to the cation vacancy or oxygen interstitial charge. For an n-type oxide, use of eqn [27] gives:

$$k' \propto [(P^i_{O_2})^{-1/n} - (P^o_{O_2})^{-1/n}] \qquad [32a]$$

where in this case n is related to the oxygen vacancy or cation interstitial charge. In most cases, the ambient oxygen pressure $P^o_{O_2}$ is much greater than $P^i_{O_2}$, which is the dissociation pressure ($P^{diss}_{O_2}$). Thus, eqns [31a] and [32a] can be approximated to give

$$k' \propto (P^o_{O_2})^{1/n} \text{ for a p-type scale} \qquad [31b]$$

and

$$k' \propto (P^i_{O_2})^{-1/n} \text{ for a n-type scale} \qquad [32b]$$

These equations show that the growth rate of a p-type oxide is directly dependent on the oxygen partial pressure in the atmosphere. By contrast, the

growth rate of an n-type oxide is independent of the external oxygen partial pressure.

Oxides formed in practice are usually more complex than what was assumed by Wagner. First, a multilayer scale can form on a number of metals, such as Fe, Cu, and Co. For instance, and as discussed earlier, a three-layered $FeO/Fe_3O_4/Fe_2O_3$ scale forms on iron above ~570 °C at atmospheric pressure. Treatments of the growth kinetics of multilayered scales have been presented by a number of authors.[27–30] In general, these treatments relate overall oxidation scaling kinetics to the intrinsic growth rates of the individual layers in the scale. Second, scales forming on metal surfaces are usually polycrystalline in structure, and in many cases, these structures are fine-grained. The activation energy for grain-boundary diffusion is lower than that for lattice diffusion by up to a factor of three. As a consequence, grain-boundary diffusion will tend to predominate at lower temperatures and can cause the scaling kinetics to be orders of magnitude higher than what would be predicted based on lattice diffusion.[26]

As indicated above, Wagner's theory considered the ideal case of scale formation in which the scale is assumed to be a compact and perfectly adherent barrier, that is, free of voids, pores, and fissures. The assumptions made by Wagner were indeed appropriate; however, deviations from Wagner's theory have been shown.[31] Many studies have shown that pores form and develop preferentially along grain boundaries in the scale.[32,33] The presence of voids in scales clearly represents a deviation from ideal scale growth. In some extreme cases, it may be necessary to take into account the void volume fraction in Wagner's model; but often the void formation may be considered to be a secondary process that does not significantly affect the overall scaling kinetics.

As the scale grows, stresses develop due to differences in the molar volume of metal and oxide(s). The resulting growth stresses are typically compressive.[34,35] More significant stresses can develop under thermal cycling conditions due to a mismatch in the coefficient of thermal expansion (CTE) between oxide scale and metal. Increasing stresses may eventually result in crack formation and even scale detachment.[35] Cracking of a protective oxide scale can result in the parabolic oxidation kinetics being interrupted by a sudden increase in rate when the gas can react directly with the metal surface. As oxide begins to cover the metal surface again, parabolic oxidation is resumed. The overall oxidation of the metal becomes approximately a paralinear process of periodic cracking and healing of a protective oxide.

1.09.3 Alloy Reactions

The fundamentals of pure-metal oxidation provide a basic understanding of alloy oxidation, but the latter is generally much more complex as a result of some, or all, of the following[14]:

(a) The various metal components in an alloy will have different affinities for oxygen, as indicated in the Ellingham diagram in **Figure 1**.
(b) More oxides may be formed, including ternary and higher oxides.
(c) A degree of solid solubility may exist between the oxides.
(d) The various metal ions will have different mobilities in the oxide phases.
(e) The various metals will have different diffusivities in the alloy.
(f) The extra degree of thermodynamic freedom provided by an additional metal component in the alloy may result in subsurface oxide precipitation (i.e., internal oxidation).

When it is considered that scales can crack, contain voids, spall, and even form multiple layers of irregular thickness, the situation becomes even more complex. The following provides a brief overview of the fundamental aspects of alloy oxidation.

1.09.3.1 Thermodynamics of Alloy Oxidation

As in the case of a pure metal, alloy oxidation is driven by an overall decrease in free energy. However, the alloy components are not in their pure state, which corresponds thermodynamically to their chemical activities being less than unity. For dilute solution of metallic component B in A, the average solvent A atom exists essentially in the same chemical surrounding environment as in its pure state, with only a small number of neighboring solute B atoms. Thus, in the limit of a very dilute solution, the A atoms follow Raoult's law,[6] such that:

$$\lim_{N_A \to 1} a_A = N_A \qquad [33]$$

where a_A and N_A are the chemical activity and mole fraction of solvent A, respectively. Also, according to Henry's law, the chemical activity of solute B is given as:

$$\lim_{N_B \to 0} a_B = \gamma_B N_B \qquad [34]$$

where γ_B is the activity coefficient of solute B for the A–B system. It can be easily shown that the dissociation P_{O_2} for an AO scale in contact with an A–B alloy is

greater than what would be calculated for AO in contact with pure A. Specifically,

$$\frac{P_{O_2}}{P^*_{O_2}} = \left(\frac{1}{a_A}\right)^2 \quad [35]$$

where a_A is the activity of A in the A–B alloy, and P_{O_2} and $P^*_{O_2}$ are the dissociation pressures for the A–B alloy and pure A, respectively.

It is typically the activity of the solute that is most important when assessing the thermodynamics of alloy oxidation; although, the results are often of limited utility. This can be shown as follows. Consider the oxidation of an A–B alloy in which the solute B forms a more stable and protective oxide. Assuming that the only stable oxides are AO and BO and that these oxides are insoluble in one another, the important reaction to consider is

$$AO + \underline{B} \rightarrow BO + \underline{A} \quad [36]$$

where $\underline{B}$ and $\underline{A}$ correspond to B and A in the alloy solution. The law of mass action for this reaction gives

$$K_{36} = \frac{a_A}{a_B} \approx \frac{N_A}{\gamma_B N_B} \quad [37]$$

Thus, reaction [36] will only proceed to the right if $\frac{a_A}{a_B} < K_{36}$, which means that there is a critical a_B, or conversely N_B, for this to occur. In most practical cases of interest, the solute–metal oxide BO is significantly more stable than the base-metal oxide AO, causing K_{36} to be much larger than unity. This, in turn, results in a very small minimum N_B value for BO to be thermodynamically stable in contact with the A–B alloy. In the case of an Ni–Cr alloy, N_{Cr} must be greater than $\sim 10^{-9}$ at 1000 °C for the displacement reaction $3NiO + 2\underline{Cr} \rightarrow Cr_2O_3 + 3\underline{Ni}$ to be thermodynamically stable.[36] Such a low Cr content is orders of magnitude below what is necessary kinetically to sustain Ni–Cr/Cr_2O_3 stability, let alone to kinetically establish a continuous Cr_2O_3 scale. For the latter, the critical Cr mole fraction, N^{crit}_{Cr}, in Ni–Cr alloy exposed to air at 1000 °C is experimentally found to be ~0.2.[37]

1.09.3.2 Criterion for the Sustained Exclusive Growth of a Protective Scale

If a continuous BO_υ scale on an A–B alloy is established under a particular set of conditions, it may be necessary to determine if its growth can be sustained under a different set of conditions. (The stoichiometric factor υ for the oxide BO_υ will be used for the remainder of this chapter in order to provide more general kinetic-based expressions.) An example of this could be the preoxidation of an alloy at a low P_{O_2} followed by in-service exposure to a higher P_{O_2} and/or different temperature. The sustained growth of a continuous BO_υ scale requires a sufficient supply of B from within the alloy to the alloy/scale interface. The resulting subsurface concentration gradient of solute B is represented schematically in **Figure 8**, in which N^i_B is the mole fraction of B in the alloy at the alloy/scale interface. The maximum possible rate of B supply in the alloy can be imposed by setting N^i_B equal to zero, thereby producing the steepest possible diffusion gradient of B. Under steady-state conditions, this maximum rate of B supply would have to equal the rate of B consumption due to BO_υ scale growth. Determination of the minimum B content in the alloy, $N^o_{B(min)}$, necessary for the sustained exclusive growth of a BO_υ scale on an A–B alloy was originally considered by Wagner,[38] who further assumed that: (1) the diffusion coefficient of B in the alloy, D_B, is independent of concentration; (2) the BO_υ scale obeys parabolic thickening kinetics with a rate constant k_p; (3) solvent metal A is insoluble in BO_υ; and (4) the recession of the alloy/scale interface may be neglected. Wagner derived the criterion

$$N^o_{B(min)} > \frac{V_m}{\upsilon M_O}\left(\frac{\pi k_p}{2D_B}\right)^{\frac{1}{2}} \quad [38]$$

where V_m is the equivalent molar volume of the alloy and M_O is the atomic weight of the oxidant, which is oxygen in this discussion ($M = 16\,g\,mol^{-1}$). Many researchers have used the criterion in eqn [38] to predict the minimum content of B necessary for a bare alloy to form an exclusive BO_υ scale layer. However, this is not a correct use of the criterion, since its derivation was based on supply rather than establishment. The

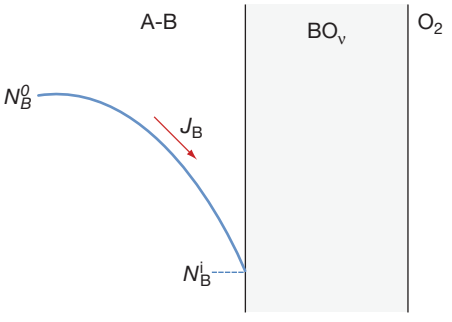

Figure 8 Schematic representation of the concentration profile of *B* in a binary alloy *A–B* which is forming an exclusive scale layer of BO_υ.

criterion given in [38] gives only the minimum possible B content in the alloy necessary to supply B at a sufficient rate to the alloy/scale interface for the sustained growth of an established BO_υ scale layer. The actual B content necessary for both the establishment and sustained growth of a BO_υ scale will very likely be higher than $N^o_{B(min)}$ owing to transient and kinetic effects.

1.09.3.3 Internal Oxidation

Internal oxidation is used here in a generic sense to represent a process in which a diffusing oxidant from the surface reacts with a less-noble solute component in the alloy to form discrete particles.[39] Internal oxidation is not desired because it changes the optimized mechanical properties of an alloy and may result in internal stress and weakening of the grain boundary.

For a dilute binary alloy A–B, the dissolved oxygen atoms can react with less-noble B atoms in the alloy in the manner,

$$\underline{B}+\upsilon\underline{O} \rightarrow BO_\upsilon \qquad [39]$$

The necessary condition for BO_υ formation in the alloy may be formulated in terms of the equilibrium solubility product K_{sp}, such that:

$$[a_B][a_O]^\upsilon > K_{sp} \qquad [40]$$

The degree to which the solubility product must be exceeded (i.e., the degree of supersaturation) before precipitation occurs depends on a number of factors, such as the stability, composition, and crystal structure of the precipitating BO_υ phase. For instance, if the crystal structure and lattice dimensions of BO_υ are such that it can form a coherent interface with the alloy matrix, then only a small degree of supersaturation is likely to be necessary for BO_υ precipitation. In general, the greater the stability of BO_υ, the lower will be its K_{sp} value. It is for this reason that the internal precipitates commonly observed in oxidized high temperature alloys are of the stable oxides Al_2O_3, SiO_2, TiO_2, and Cr_2O_3.[40,41] Multiple internal oxidation zones can also develop if more than one reaction product is stable.[42,43] The sequence of the thermodynamically possible phases progresses from metal-rich in the innermost zone of the alloy to oxidant-rich at the surface.

The internal oxidation zone extends to the depth at which the activity of dissolved oxygen becomes too small for the formation of the oxide BO_υ. The kinetics of internal oxidation are generally found to be diffusion-controlled and the depth of the internal oxidation zone, ξ, in an alloy undergoing no external scale formation can be described by the following kinetic expression, assuming no enrichment of B in the internal oxidation zone[44,45]:

$$\xi = \left(\frac{2N^s_O D_O t}{\upsilon N^o_B}\right)^{1/2} \qquad [41]$$

where N^s_O is the solubility of the oxidant in the alloy, D_O is the diffusivity of the oxidant in the alloy, N^o_B is the initial solute concentration in the A–B alloy, and t is the time. The product $N^s_O D_O$ is the oxygen permeability in alloy. The solubility of oxygen in the alloy depends upon the oxygen partial pressure at the alloy surface in accordance with Sievert's law,[6] that is,

$$N^s_O \propto P^{1/2}_{O_2} \qquad [42]$$

Thus, the depth of internal oxidation would be expected to decrease with decreasing P_{O_2} in the manner $\xi \propto P^{1/4}_{O_2}$.

The above discussion considers only internal precipitation in the absence of external scale formation. In the case of AO_υ scale formation, the value of N^s_O is no longer fixed by the environment but is instead fixed by the equilibrium between at the alloy/scale interface (assuming no through-scale access by the oxidant) according to the reaction,

$$\underline{A}+\frac{\upsilon}{2}O_2 = AO_\upsilon \qquad [43]$$

The effective thickness of the internal precipitation zone in the situation of concurrent AO_υ-scale formation decreases in a most pronounced manner from that predicted in the absence of an external scale at large k_p and N^o_B values.[46] A large k_p value for AO_υ-scale growth corresponds to a large amount of metal recession, which means the total attack is still high, even though the internal precipitation zone is relatively low.

The preceding theoretical considerations are based on models assuming predominant lattice diffusion of both oxygen and the alloying element. As such, the theoretical treatments are only expected to apply to relatively high temperatures or to very large-grained materials, with the extreme being single crystals. As the temperature is reduced, grain-boundary effects will become increasingly important. This is due to relatively rapid diffusion along grain boundaries, enhanced concentration or segregation of the oxidant and the alloying element at grain boundaries, and a preferred tendency for nucleation at grain boundaries.[4]

1.09.3.4 Transition from Internal Oxidation to External Scale Formation

The transition from internal to external oxide formation typically occurs with a relatively small increase in the alloy content of the less-noble component B in the A–B alloy, at which oxidation leads to the formation of a surface scale of BO_υ, and the alloy no longer undergoes internal oxidation. Considering again the alloy system A–B, there are two limiting possible situations: one is when only one of the components can oxidize and the other is when both of the components can oxidize. For the first case, if the oxygen partial pressure is low (i.e., below the stability of AO_υ formation), the component B in the alloy surface nucleates as BO_υ in an A-rich matrix. If B can diffuse fast enough to reach the surface and maintain a sufficient supply for BO_υ formation, a complete surface layer of BO_υ will be established. However, if this condition is not met, then BO_υ will precipitate as internal particles within the alloy. So, the internal or external formation of BO_υ depends on the balance between the outward flux of B and the inward flux of atomic oxygen into the alloy.

Wagner[47] proposed that the condition for the transition from internal to external BO_υ formation occurs when a critical volume fraction of BO_υ, f^*, is attained. Under this condition, the influx of oxygen is so restricted that sideways growth of the internal BO_υ precipitates is kinetically favored to the extent that BO_υ eventually forms as a continuous layer on the alloy surface. Under conditions of no or a negligibly small rate of metal recession, the following criterion for the transition from internal to external BO_υ formation was obtained:

$$N_{B^*}^{o} \geq \left[f^* \left(\frac{V_m}{V_{ox}} \right) \pi \frac{N_O^S D_O}{2 \upsilon D_B} \right]^{1/2} \qquad [44]$$

where $N_{B^*}^{o}$ is the critical mole fraction of B in the alloy, V_m is molar volume of the alloy, V_{ox} is molar volume of the oxide, and D_B is the diffusion coefficient of solute B in the alloy. Rapp[44] reported excellent agreement between experimental and reasonably predicted values of $N_{In^*}^{o}$ as a function of oxygen partial pressure in Ag–In alloys oxidized at 550°C. The value of f^* is usually taken to be 0.3 in accordance with the results from this study by Rapp.

From the criterion given by eqn [44], it is seen that $N_{B^*}^{o}$ can be decreased by decreasing the product of N_O^s and D_O (i.e., decreasing the permeability of oxygen) and/or increasing D_B. Indeed, the direct and indirect control of these variables in numerous experimental studies conducted over the past 40 years have validated this criterion.[1]

1.09.4 Epilogue

Advances in the high temperature stability of materials are critically needed to realize the full performance and potential of many current and future commercial systems. These advances must lead to significantly enhanced capabilities that will allow high temperature components to operate robustly for prolonged periods in harsh environments, such as those involving aggressive gases, deposits, photon or radiation fluxes, stresses, high or low pressures, or some combination of these conditions. For example, coal gasification, biomass conversion, and gas-cooled nuclear reactor systems typically produce complex, multioxidant gaseous environments that can be highly aggressive from the standpoint of surface degrading structural components. The resulting multioxidant process environments are often non-equilibrium and can involve both gaseous and deposit-induced attack. Fundamentally, the high temperature stability of a material in an aggressive environment relates to reactions and transport at and across its external surfaces. Similar to what was discussed in this chapter, these reactions are defined in terms of some combination of chemical potential, temperature and pressure and can be highly complex. Different processes, many of them coupled, are involved from the onset of reaction, that is, the absorption and dissociation of gaseous molecules at the surface, to the steady-state growth of a protective surface scale that develops. Indeed, the ability to control the growth and stability of this scale and to predict its behavior under different types of extreme chemical environments for extended periods of time will require a much greater basic understanding of the underlying reactions and transport processes involved. The basic starting points have been presented in this chapter, but still much more research and development are needed to improve the reliability and durability of materials exposed to aggressive conditions.

References

1. Gleeson, B. In *Corrosion and Environmental Degradation, Vol. II:* Volume 19 of the Materials Science and Technology Series; Schütze, M., Ed.; Wiley-VCH: Weinheim, Germany, 2000.

2. Lai, G. Y. *High-Temperature Corrosion of Engineering Alloys;* ASM International: Materials Park, OH, 1990.
3. Kofstad, P. *High Temperature Oxidation of Metals*; John Wiley and Sons: New York, 1966.
4. Young, D. *High Temperature Oxidation and Corrosion of Metals*; Elsevier: Amsterdam, 2008.
5. Alcock, J. C. B.; Easterbrook, E. Thermodynamics and Kinetics of Gas-Metal Systems. In *Corrosion, Volume 1: Metal/Environment Reactions*, 3rd ed.; Shreir, L. L., Jarman, R. A., Burstein, G. T., Eds.; Butterworth-Heinemann: London, 1994.
6. Gaskall, D. R. *Introduction to the Thermodynamics of Materials*, 4th ed.; Taylor & Francis: New York, 2008.
7. Kubaschewski, O.; Alcock, C. B. *Metallurgucal Thermochemistry*, 5th ed.; Pergamon Press: Oxford, 1979.
8. Barin, I.; Platzki, G. *Thermochemical Data of Pure Substances*; VCH: Weinheim, 1995.
9. JANAF Thermochemical Data, Army-Navy-Air Force Thermochemical Panel, Dow Chemical Company, Midland, MI, 1962–1963.
10. Lou, V. L. K.; Mitchell, T. E.; Heuer, A. H. *J. Am. Ceram. Soc.* **1984**, *68*, 49.
11. Giggins, C. S.; Pettit, F. S. *Oxid. Met.* **1980**, *14*, 363.
12. Stroosnijder, M. F.; Quadakkers, W. J. *High Temp. Technol.* **1986**, *4*, 141.
13. LaBranche, M. H.; Yurek, G. J. *Oxid. Met.* **1987**, *28*, 73.
14. Birks, N.; Meier, G. H. *Introduction to High Temperature Oxidation of Metals*; Edward Arnold: London, 1983.
15. Peraldi, R.; Monceau, D.; Pieraggi, B. *Oxid. Met.* **2002**, *58*, 275.
16. Naumenko, D.; Gleeson, B.; Wessel, E.; Singheiser, L.; Quadakkers, W. J. *Metall. Mater. Trans. A* **2007**, *38A*, 2974.
17. Lee, V. H. J.; Gleeson, B.; Young, D. J. *Oxid. Met.* **2005**, *63*, 15.
18. Bradford, S. A. Fundamentals of Corrosion in Gases. In *Metals Handbook*, 9th ed.; *Corrosion;* ASM International: Metals Park, OH, 1987; Vol. 13.
19. Pettit, F. S.; Wagner, J. B. *Acta Met.* **1964**, *12*, 35.
20. Sheasby, J. S.; Smeltzer, W. W. *Oxid. Met.* **1981**, *15*, 215.
21. Kofstad, P. *Nonstoichiometry, Diffusion and Electrical Conductivity in Binary Metal Oxides*; Wiley-Interscience: New York, 1972.
22. Giggins, C. S.; Pettit, F. S. *Trans. AIME* **1969**, *245*, 2495.
23. Wagner, C. *Z. Phys. Chem.* **1933**, *21*, 25.
24. Wagner, C. *Atom Movements*; ASM: Cleveland, 1951; p 153.
25. Raynaud, G. M.; Clark, W. A. T.; Rapp, R. A. *Metall. Trans. A* **1984**, *15A*, 573.
26. Atkinson, A. *Rev. Mod. Phys.* **1985**, *57*, 437.
27. Garnaud, G.; Rapp, R. A. *Oxid. Met.* **1977**, *11*, 193.
28. Hsu, H. S. *Oxid. Met.* **1986**, *26*, 315.
29. Gesmundo, F.; Viani, F. *Corros. Sci.* **1978**, *18*, 217.
30. Wang, G.; Gleeson, B.; Douglass, D. L. *Oxid. Met.* **1989**, *31*, 415.
31. Yurek, G. J. *Corrosion Mechanisms*; Marcel Dekker Inc.: New York, 1987; p 397.
32. Dravinieks, A.; McDonald, H. *J. Electrochem. Soc.* **1948**, *94*, 139.
33. Mrowec, S. In *Proceedings of JIM International Symposium on High Temperature Corrosion of Metals and Alloys;* Mt Fuji, Japan, 17–20 November 1982; p 115.
34. Stringer, J. *Corros. Sci.* **1970**, *10*, 1970, 513.
35. Schütze, M. *Protective Oxide Scales and Their Breakdown*; Institute of Corrosion and Wiley Series on Corrosion and Protection; John Wiley & Sons Ltd: England, 1991.
36. Birks, N.; Rickert, H. *J. Inst. Met.* **1963**, *91*, 1963, 308.
37. Wood, G. C.; Wright, I. G.; Hodgkiess, T.; Whittle, D. P. *Werkst. Korros.* **1970**, *20*, 900.
38. Wagner, C. *J. Electrochem. Soc.* **1952**, *99*, 369.
39. Douglass, D. L. *Oxid. Met.* **1995**, *44*, 81.
40. Gleeson, B.; Harper, M. A. *Oxid. Met.* **1998**, *49*, 373.
41. Wei, F. I.; Stott, F. H. *High Temp. Technol.* **1989**, *7*, 59.
42. Schnaas, A.; Grabke, H. J. *Oxid. Met.* **1978**, *12*, 387.
43. Kane, R. H. *Corrosion* **1981**, *37*, 187.
44. Rapp, R. A. *Corrosion* **1965**, *21*, 382.
45. Wagner, C. *Z. Elektrochem.* **1959**, *63*, 772.
46. Gesmundo, F.; Viani, F. *Oxid. Met.* **1986**, *25*, 269.
47. Wagner, C. *Z. Elektrochem.* **1959**, *63*, 772.